Integrated Porous Cu Host Induced High-Stable Bidirectional Li Plating/Stripping Behavior for Practical Li Metal Batteries

Jianyu Chen, Sijia Li, Xin Qiao, Yizhou Wang, Linna Lei, Zhiyang Lyu, Jin Zhao, Yu Zhang, Ruiqing Liu, Qinghua Liang, and Yanwen Ma**

Dr. J. Chen, S. Li, X. Qiao, L. Lei, Prof. J. Zhao, Dr. R. Liu, Prof. Y. Ma

Key Laboratory for Organic Electronics and Information Displays, Jiangsu Key Laboratory for Biosensors, Institute of Advanced Materials (IAM), Jiangsu National Synergetic Innovation Center for Advanced Materials (SICAM), Nanjing University of Posts & Telecommunications, 9 Wenyuan Road, Nanjing 210023, China.

E-mail: iamjzhao@njupt.edu.cn, iamywma@njupt.edu.cn.

Y. Wang

Materials Science and Engineering, King Abdullah University of Science and Technology (KAUST), Thuwal 23955-6900, Saudi Arabia.

Dr. Z. Lyu

Jiangsu Key Laboratory for Design and Manufacture of Micro-Nano Biomedical Instruments, School of Mechanical Engineering, Southeast University, Nanjing, 211189, China

Dr. Y. Zhang

Jiangsu Collaborative Innovation Centre of Biomedical Functional Materials, Jiangsu Key Laboratory of New Power Batteries, College of Chemistry and Materials Science, Nanjing Normal University, Nanjing 210023, China.

Dr. Q. Liang

Department of Chemical Engineering, The University of Melbourne, Parkville, VIC 3010, Australia.

This is the author manuscript accepted for publication and has undergone full peer review but has not been through the copyediting, typesetting, pagination and proofreading process, which may lead to differences between this version and the Version of Record. Please cite this article as doi: 10.1002/smll.202105999.

Keywords: Li metal anode, current collector, through-pore structure, bidirectional plating/stripping, pouch cell

Abstract

The double-sided coated electrodes with active materials are widely used for commercial Li-ion batteries with a higher energy density. Accordingly, developing an anode current collector that can accommodate the stable and homogeneous Li plating/stripping on both sides will be highly desired for practical Li metal batteries (LMBs) with better performance. Herein, an integrated bidirectional porous Cu (IBP-Cu) film with a through-pore structure is fabricated as high-performing Li metal hosts using the powder sintering method. The resultant IBP-Cu current collector with tunable pore volume and size exhibits high mechanical flexibility and stability. The bidirectional and through-pore structure enables the IBP-Cu host to achieve homogeneous Li metal deposition and effectively suppresses the dendritic Li growth. Impressively, the as-fabricated Li/IBP-Cu anode exhibits a remarkable capacity of up to 7.0 mAh cm^{-2} for deep plating/stripping, outstanding rate performance, and ultralong cycling ability with high Coulombic efficiency of ~100% for 1000 cycles. More practicably, a designed pouch cell coupled with one Li/IBP-Cu anode and two $LiFePO_4$ cathodes exhibits a highly elevated energy density (~187.5%) compared with a pouch cell with one anode and one cathode. Such design of a bidirectional porous Cu current collector with stable Li plating/stripping behaviors suggests its promising practical applications for next-generation Li metal batteries.

1. Introduction

The specific energy density of the state-of-the-art Li-ion batteries based on graphite anodes has almost reached the theoretical limit (~350 Wh kg^{-1}), which is still far below the increasing

requirement of high-energy-density applications.[1-5] Among various anode materials, Li metal is regarded as the ultimate anode material due to its high theoretical specific capacity (3860 mAh g^{-1}) and low redox potential (-3.04 V versus standard hydrogen electrode).[6-13] This motivates the intense research efforts in next-generation batteries, such as Li-S, Li-O_2, Li-CO_2 batteries.[14-21] However, the commercialization of the Li metal anode is still hindered by its huge volumetric change and uncontrolled dendrite growth during the repeated plating/stripping. These drawbacks will cause a series of issues, e.g., irreversible capacity loss, low Coulombic efficiency (CE), internal short circuits, and even battery explosion.[22-26] To address these issues, considerable efforts have been focused on optimizing electrolytes,[27-31] introducing artificial SEI layers,[32-37] modifying separators,[38-41] and designing nanostructures.[42-45] However, the fundamental problem of Li dendrite growth remains to be solved as Li metal anodes are operated under high current densities and deep plating/stripping cycling.[46-49] Thus, developing an easy approach to overcome volume expansion and achieve dendrite-free Li anodes with high stability at high current density and deep plating/stripping conditions is of great significance.

Porous hosts with optimized mass and charge transport behaviors have been widely developed to enable uniform Li deposition and mitigate the stress and volume change of Li metal anode.[50-54] Among the reported hosts for Li metal, 3D porous Cu is regarded as a promising host for stabilizing Li since Cu is the commercialized current collector for Li-ion batteries and its 3D porous structure can effectively regulate the deposition behavior of Li

metal. Up to now, tremendous progress has been made for the mechanisms of preventing Li dendrite growth by employing 3D porous Cu films as current collectors for Li metal anodes, including providing a large electroactive surface area, decreasing local current density, and affording sufficient diffusion channels to enable the ions transport.[55-61] Overall, the porous structure of the Cu current collector plays the most important role in the above-mentioned working mechanisms. Optimizing and modulating the porous structure of the Cu host will be desired for further improving the overall electrochemical performance for Li metal anodes. However, the current previously reported 3D porous Cu for Li metal batteries only used one side to accommodate Li plating/stripping. We assumed that it will be practicable to use powder sintered porous Cu as a bidirectional Li plating/stripping host to make full use of the through-pore structure feature of the porous Cu, i.e., use one anode coupled with two cathodes since such a design can greatly reduce the mass ratio of the current collector in Li metal anode and increase the energy density of the batteries.

Enlighten by that powder sintering is a facial method for fabricating 3D porous Cu with tunable porosity,[62, 63] we here fabricated an integrated bidirectional porous (IBP-Cu) current collector with the tunable through-pore structure for ultrastable Li metal anode through sintering Cu micropowders. Impressively, the IBP-Cu incorporated with Li (Li/IBP-Cu) exhibits extraordinary structure stability over 4000 h under 1.0 mA cm^{-2} and 1.0 mAh cm^{-2} in the symmetric cell. Even under an extremely deep plating/stripping condition (7.0 mAh cm^{-2}), Li/IBP-Cu anode shows good cycling stability with high Coulombic efficiency of ~100% for 100

cycles. By coupling with $LiFePO_4$ (LFP) or S cathode, the coin cells with Li/IBP-Cu anode show significantly improved electrochemical performance in capacity, rate capability, and cycling performance compared to the cells with Li/planar Cu (Li/PL-Cu) anode. Most importantly, the LFP|Li/IBP-Cu|LFP pouch cell using IBP-Cu as bidirectional current collector significantly increases the anode utilization and result in an improvement of ~187.5% for the energy density than the LFP|Li/IBP-Cu pouch cell. The electrochemical performance of IBP-Cu as host for Li metal anode is among the best for the reported porous Cu current collector. Such an easy and scalable method for fabricating integrated bidirectional porous Cu film as the current collector for a homogeneous Li deposition not only suggests the feasibility of bidirectional porosity design for high-performing Li metal anode but also demonstrates its great potential for future applications.

2. Results and Discussion

The assumed plating and stripping processes of metallic Li on planar Cu, unidirectionally porous Cu, and IBP-Cu current collectors are schematically illustrated in **Fig. 1**. Owing to the disorder and isolated nucleation site of the planar surface, dendritic Li tends to grow on PL-Cu after the repeated plating/stripping. For the unidirectionally porous Cu, i.e. the dense Cu substrate with porous surface, its dense inner structure is not favorable for high current collector utilization and will result in a low mass loading of Li. In contrast, the IBP-Cu current collector is favorable for bidirectional stable Li plating/stripping due to the through-pore architecture with high surface area and well-distributed pores. Besides, the highly porous

structure is beneficial for reducing the host mass. To study the influence of pore structure on Li deposition behavior, COMSOL Multiphysics was conducted to simulate the current density and Li^+ concentration distribution (Figure 1b,c,d). The current density on the IBP-Cu current collector is lower than the planar Cu (PL-Cu) because of the larger outer and inner surface area of the porous Cu skeleton (Fig. S1). In addition, the current density in the inner porous Cu skeleton is much larger than that on the outer surface, resulting in preferential nucleation and deposition of Li inside the skeleton. Besides, the IBP-Cu also shows better wettability than the PL-Cu, which should be ascribed to the porous structure (Figure S2, S3). According to the first *Fick's law* and *Poisson's* equation, the diffusion flux of Li^+ near the current collector surface is relative to the electric field and the concentration gradient of Li-ion (Figure 1d).[61] The IBP-Cu shows a more homogeneous Li^+ diffusion path, concentration distribution, and electric field than the PL-Cu, which is favorable for the uniform Li deposition and better electrochemical performances.

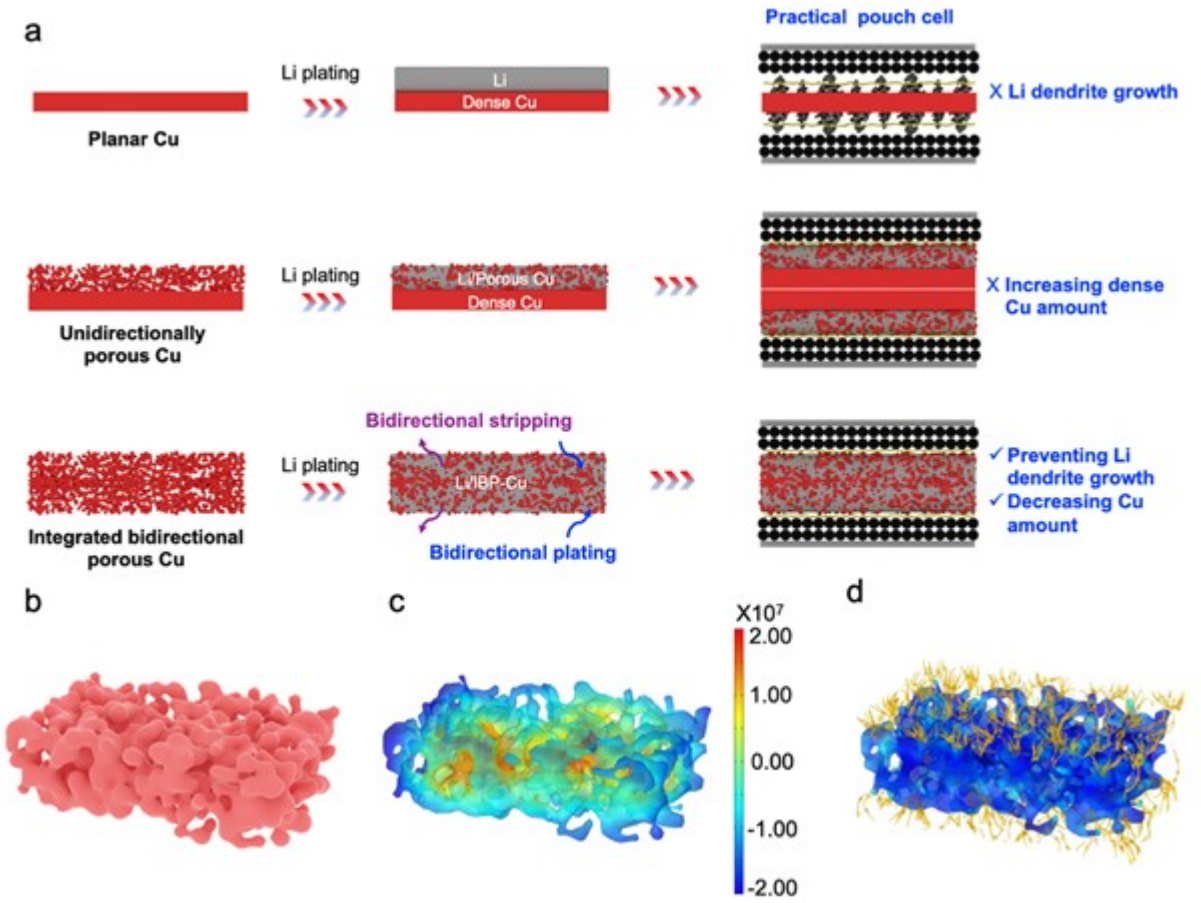

Figure 1. Schematic illustration of the effects for three different current collectors on Li plating/stripping behavior. (a) Schematic of Li plating/stripping process on the PL-Cu, unidirectional porous Cu, and IBP-Cu current collectors during cycling; schematic diagram for the designed IBP-Cu model (b) and the corresponding current density (c) and Li-ion concentration (d) distribution in it.

Powder sintering is a facile and low-cost method to fabricate flexible IBP-Cu on a large scale (**Figure 2**a,b). The color of the Cu micropowders changes from brick red to light pink after sintering (Figure S4), indicating the reduction of the oxide layer. This is verified by XRD patterns (Figure 2c). Sintering temperatures from 600 to 900 °C were applied to control the IBP-Cu current collector with optimized morphology and pore structure. Notably, the Cu particles can be fully integrated for producing a free-standing film at 750 °C. With increasing the sintering

temperature, the sintering neck grows gradually (Figure S5). Meanwhile, the Cu particles merged as a result of the highly decreased porosity (Figure S6). The ink penetration and diffusion experiments also reveal the porosity evolution of IBP-Cu obtained under different temperatures. The ink can only filter through the IBP-Cu obtained below 800 °C, indicating the through-pore structure for the IBP-Cu obtained below this temperature (Figure S3). Under an optimized sintering temperature of 750 °C, the resultant IBP-Cu exhibits a well interconnected through-pore structure with a porosity of 45.19%. Such a highly porous structure is favorable for reducing the mass of the current collector and accelerating the lithium-ion transfer (Figure 2d,e,f).[56, 60] The interconnected structure also enables the IBP-Cu with a highly enhanced mechanical property and high structural stability (Figure S7). Moreover, the interconnected through-pore structure of IBP-Cu can be well maintained after changing the thickness (Figure S8). The pore volumes for IBP-Cu film with a thickness of 100 µm obtained at 600, 700, 750, 800, and 900 °C are 0.131, 0.067, 0.054, 0.053, and 0.003 $cm^3 g^{-1}$, respectively (Figure S9). The pore size for IBP-Cu obtained at different temperatures are all located at around 1 to 100 µm regardless of the thickness change (Figure S10**)**. The areal capacity density of the Li metal accommodated in IBP-Cu with a thickness of 100 µm obtained at 750 °C is estimated to be ~7.77 mAh cm^{-2} (Table S1). Such an areal capacity density can fulfill most of the present high Li loading demands and can be improved by further increasing the thickness of the IBP-Cu.[49, 50, 55, 56]

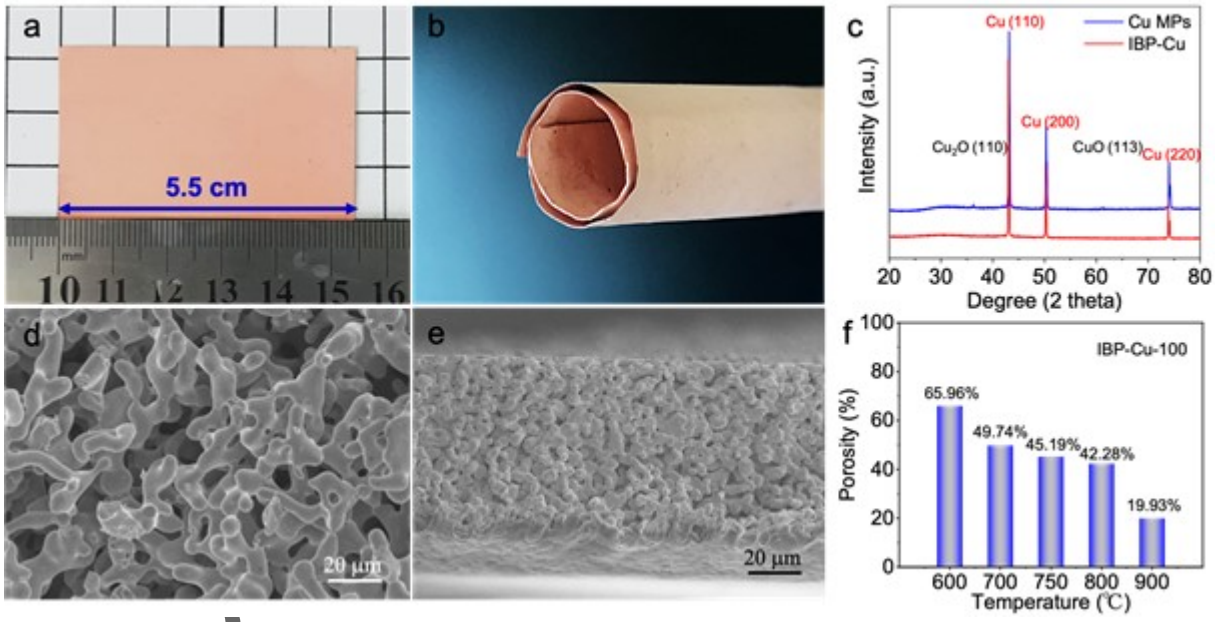

Figure 2. Morphological and structural characterizations of IBP-Cu current collectors. (a, b) Photographs of the large-scaled IBP-Cu electrodes; (c) XRD patterns of Cu micropowders before and after sintering; (d, e) SEM image for top-view (d) and cross-section view (e) of IBP-Cu obtained under 750 ˚C; (f) porosity of IBP-Cu electrodes prepared at 600 to 900 ˚C with the thickness of 100 μm.

The IBP-Cu film with a thickness of 100 μm obtained at 750 °C was specially acquired for the following measurements due to the well-interconnected through-pore and the highest areal capacity density of 7.77 mAh cm^{-2} for Li deposition (Figure 2d,e and Table S1). To investigate the Li plating/stripping behavior and structural reversibility of IBP-Cu, *ex-situ* SEM observations of IBP-Cu were carried out under different galvanostatic discharge/charge states (**Figure 3** and Figure S11). Figure 3a shows the 1st and 100th plating/stripping voltage profiles of the Li/IBP-Cu half-cell at different discharge/charge states, as marked in Figure 3b-i and Figure S11a-h. As can be seen from Figure 3b-3f and Figure S11a-e, the interconnected through-pore of the pristine IBP-Cu was gradually filled by the deposited Li with increasing the

discharging time range from 1 to 7 h and finally, resulting in a smooth Li deposition morphology and an excellent deep plating/stripping performance (7.0 mAh cm^{-2}, ca. 90 % of the theoretical maximum Li accommodation capacity). The homogeneous Li plating behavior is ascribed to the interconnected through-pore induced homogeneous Li^+ diffusion path, concentration distribution, and electric field (Figure 1c,d and Figure S11b,c). After the deposited Li was entirely stripped out from IBP-Cu, its initial porous skeleton maintains (Figure 3b,g and Figure S11a,f), indicating the high reversibility of the IBP-Cu current collector during Li plating and stripping. The homogeneous Li plating behavior and well-interconnected through-pore of IBP-Cu still be well maintained even after cycling for 100 cycles, further confirming the homogeneous Li plating behavior and high structural reversibility of IBP-Cu (Figure 3h,i and Figure S11g,h).

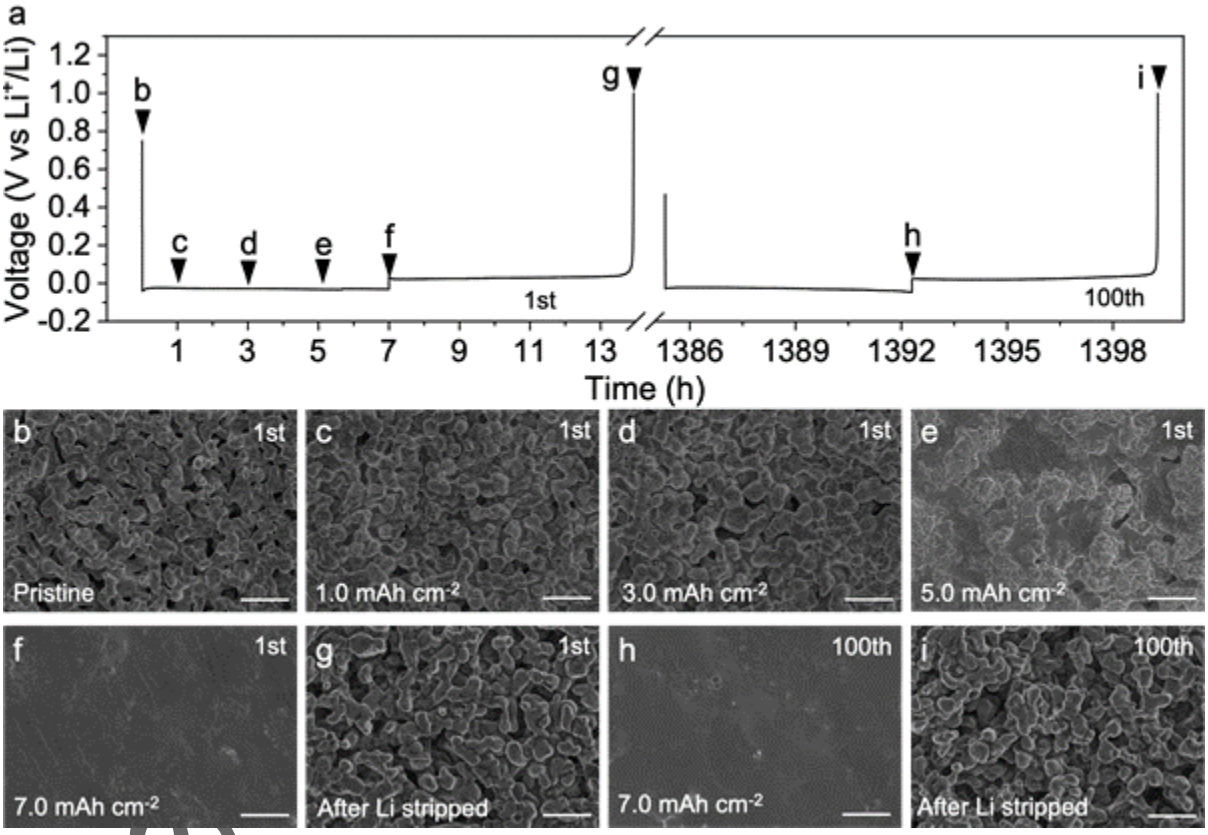

Figure 3. Li metal plating/stripping behavior in IBP-Cu host. (a) Electrochemical plating/stripping voltage profile of IBP-Cu half-cell conducted at 1.0 mA cm^{-2}. (b-g) Top-view SEM images of IBP-Cu for the 1st cycle under the pristine states (b), a plating capacity of 1.0 mAh cm^{-2} (c), 3.0 mAh cm^{-2} (d), 5.0 mAh cm^{-2} (e), 7.0 mAh cm^{-2} (f), and fully-stripped (g). (h, i) Top-view SEM images of IBP-Cu for the 100th cycle under plating capacity of 7.0 mAh cm^{-2} (h) and fully-stripped (i).

The electrochemical performances of IBP-Cu and PL-Cu as a current collector for Li plating were first investigated by fabricating half-cells (**Fig. 4a**, Figs. S12 and S13). The initial CE of the Li/IBP-Cu anode is 94.6% due to the stable and thin SEI layer formed on the surface of IBP-Cu. The half-cell test of the Li/IBP-Cu anodes can run stably for 1000 cycles at a current density of 1 mA cm^{-2} and a cycling capacity of 1 mAh cm^{-2}, the corresponding CEs > 99% can be obtained during the long-term cycling process (Fig. 4a). The high coulombic efficiency in this study is attributed to the following reasons: (1) the IBP-Cu electrode was pretreated by cycling from 0

to 1 V at 50 μA cm^{-2}, which can remove the impurities on the current collector surface and enable the formation of a stable SEI film in advance; (2) the relative large specific surface of IBP-Cu electrode can effectively reduce the local current density of the electrode, thus favorable for a thin and uniform SEI layer formation; (3) the high conductivity of the IBP-Cu electrode is beneficial for charge transfer, which also favors the formation of a thin and uniform SEI layer; (4) the IBP-Cu current collectors can effectively suppress the growth of dendrites, which ensures the long lifespan of the battery. The η_n (nucleation overpotential) of the IBP-Cu current collector presented at the first cycle is 36 mV, which is much smaller than 52 mV for the PL-Cu current collector, suggesting the lower Li nucleation obstacle for IBP-Cu (Fig. S12b). To study the effect of deposition amount of Li with pore volume, different thicknesses of IBP-Cu current collectors were tested in the half-cell. As shown in Fig. S14, the CEs of IBP-Cu-25 to IBP-Cu-500 can achieve 97.9%, 97.3%, 94.6%, 91.6%, 88.9 %, 83.48%, and 73.7% for the 1st cycle, respectively. The CE values for the first cycle decrease with increasing the thickness of the IBP-Cu. When the thickness increases to > 300 μm, the obtained CE of these current collectors drop and exhibit poor electrochemical stability during the long-term cycling, suggesting irreversibility due to the inferior ion and electron diffusion when the thickness is too large. Hence, the optimal thickness of IBP-Cu should be below 200 μm to achieve better electrochemical performance.

Symmetric cells were assembled to study the Li plating/stripping behavior in IBP-Cu and PL-Cu current collectors (Figs. 4b, c, and Fig. S15). As expected, Li/IBP-Cu based symmetric cell

exhibits a low and stable polarization voltage of ~46 mV for over 4000 h at 1.0 mA cm^{-2} and 1.0 mAh cm^{-2}. In contrast, Li/PL-Cu symmetric cell shows a large voltage fluctuation and sudden voltage drop at around 460 h, which refers to the internal cell short-circuits caused by Li dendrites (Fig. 4b). At the current densities range from 1.0 to 50.0 mA cm^{-2} with a fixed areal capacity of 1.0 mAh cm^{-2}, Li/IBP-Cu based symmetric cell also exhibits the much higher rate capability, lower overpotentials, and longer cycling stability than those for the symmetric cell based on Li/PL-Cu (Fig. S15). The lower electrochemical polarization for IBP-Cu than PL-Cu is attributed to the following two reasons. Firstly, the continuous conductive skeleton of IBP-Cu with a large surface area is favorable for reducing the Li nucleation resistance. Secondly, the abundant protuberant tips in IBP-Cu can act as the charge centers and nucleation sites for the uniform Li deposition.

By varying the current density from 0.1 to 6.0 mA cm^{-2} with a fixed Li plating/stripping time of 1 h, the polarization voltage of IBP-Cu based symmetric cells is 10, 16, 20, 28, 40, and 73 mV at the corresponding current densities of 0.1, 0.2, 0.5, 1.0, 2.0, and 3.0 mA cm^{-2}. Even under a deep plating/stripping condition (6.0 mAh cm^{-2}), the symmetric cells based on IBP-Cu still exhibit a steady voltage hysteresis of 115 mV and show no evidence of a dendrite-induced failure. This is in sharp contrast to the much higher overpotential, lower rate capability, and shorter cycle life observed for PL-Cu based symmetric cell, demonstrating the superiority in deep plating/stripping stability of Li/IBP-Cu over Li/PL-Cu based symmetric cell (Fig. 4c). Such a good performance of IBP-Cu for Li plating/stripping is even superior to most of the other 3D

Cu-based Li metal anodes (Table S2). The superiority of IBP-Cu over PL-Cu as Li anode host was further examined by coupling with $LiFePO_4$ (LFP) and S as cathodes. The coin cell for both Li|LFP or Li|S systems with Li/IBP-Cu anodes always shows a much higher capacity and longer cycling stability than those with Li/PL-Cu anodes (Figs. S16-S18).

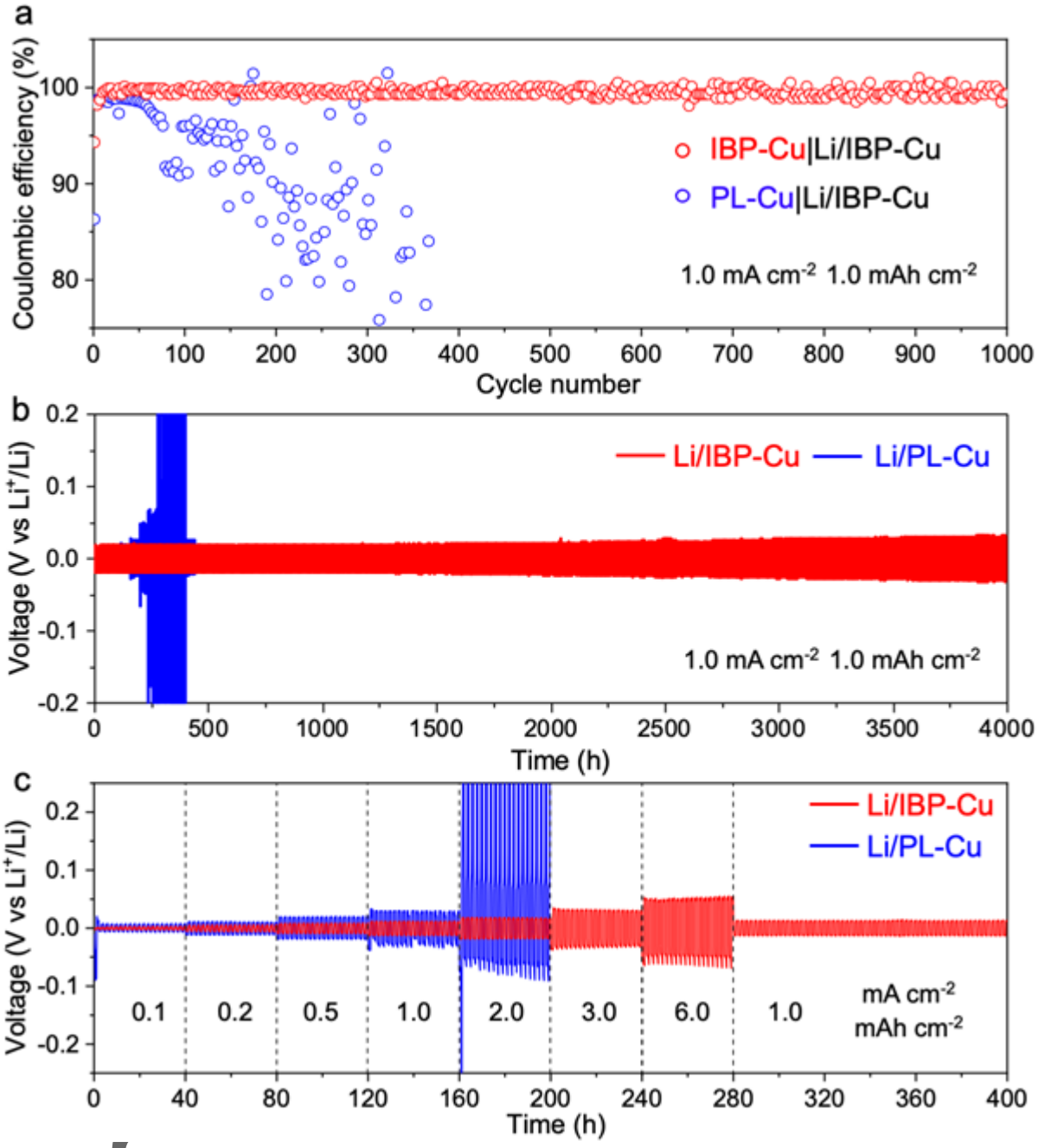

Figure 4. Electrochemical performance of Li/IBP-Cu electrodes. (a) CEs of the Li plating/stripping on the IBP-Cu current collector at 1.0 mA cm^{-2} and 1.0 mAh cm^{-2}. (b) Voltage profiles of Li/IBP-Cu and Li/PL-Cu based symmetric cells at 1.0 mA cm^{-2} with fixed plating/stripping time of 1 h; (c) Rate performance of the Li/IBP-Cu and Li/PL-Cu based symmetric cells at different current densities and areal capacity.

The feasibility of IBP-Cu as the bidirectional porous current collector for Li metal battery

was evaluated in LFP|Li/IBP-Cu|LFP pouch cell. As depicted in **Fig. 5**a, the pouch cell was fabricated by sandwiching one Li/IBP-Cu anode between two LFP cathodes. Such a design can significantly increase the utilization of an anode current collector compared with the cell with one anode coupled with one cathode. This is favorable for improving the energy density by reducing the mass of the anode (Figs. S19 and S20). The initial capacity of the LFP|Li/IBP-Cu|LFP pouch cell is 163.0 mAh g^{-1} at 1 C, almost the same as the value of 154.0 mAh g^{-1} in a typical coin cell and the value of 163.8 mAh g^{-1} in LFP|Li/IBP-Cu pouch cell (Fig. 5b, Figs. S16, and S21). After 100 cycles, the capacity retention of LFP|Li/IBP-Cu|LFP pouch cell is ~86.8 % (141.5 mAh g^{-1}). Besides the initial several activation cycles, the CE for LFP|Li/IBP-Cu|LFP pouch cell retains ~100% during the following cycling process (Fig. 5c). Furthermore, the LFP|Li/IBP-Cu|LFP pouch cell delivers a much higher gravimetric energy density of 58.65 Wh kg^{-1} than the LFP|Li/IBP-Cu pouch cell (31.28 Wh kg^{-1}). The significant improvement of energy density (187.5%) is ascribed to the increased utilization of the anode current collector (Figs. S19, S20 and Table S3). Our demo experiments show that a timer can be powered by one LFP|Li/IBP-Cu|LFP pouch cell under both flat and bending states (Figs. 5d,e). Moreover, the timer can work for over 96 hours powered by the LFP|Li/IBP-Cu|LFP pouch cell, indicating the potential of the IBP-Cu current collector for practical applications Figure. 5f-g and Fig. S22).

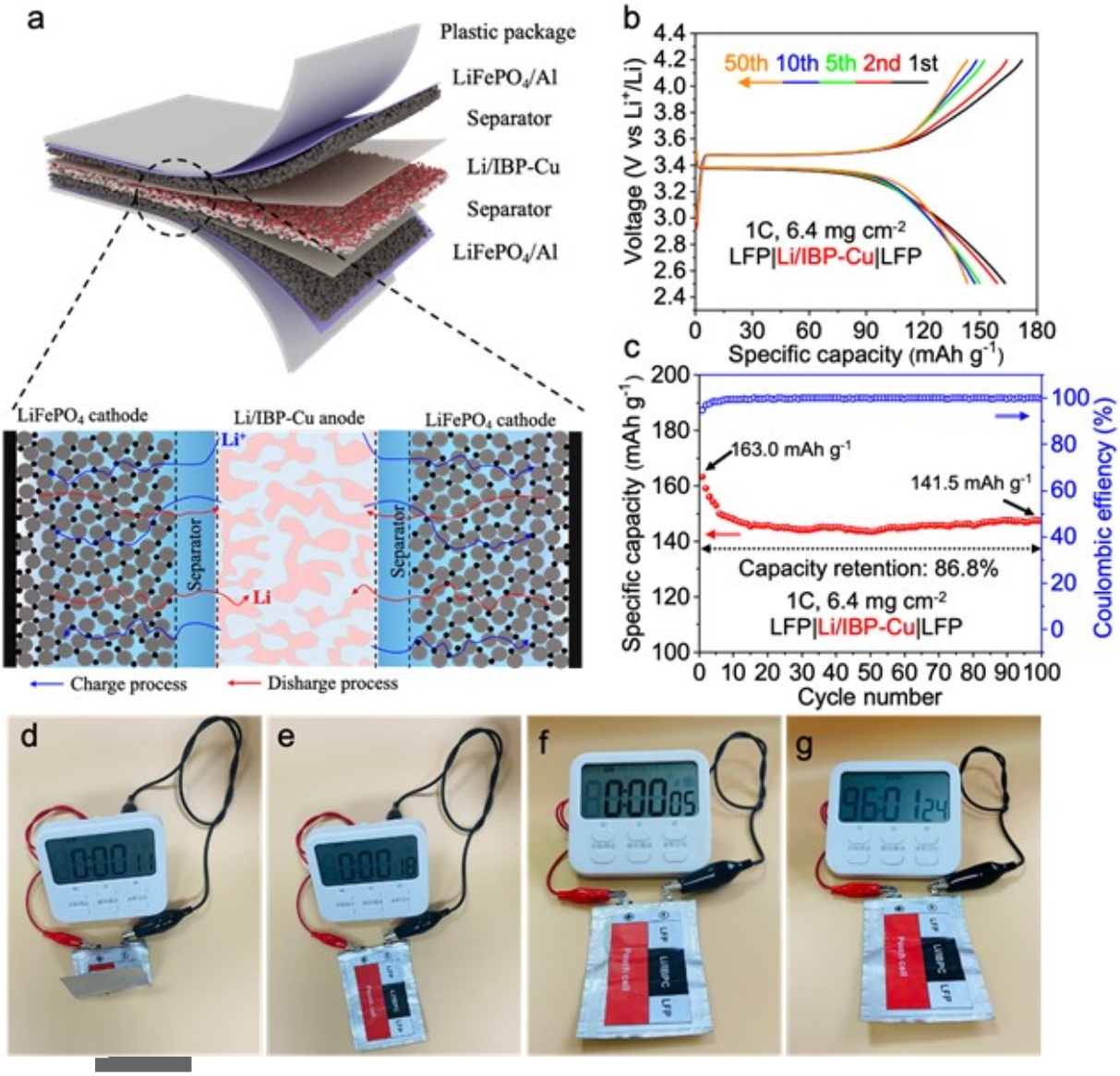

Figure 5. Practical pouch cell performance. (a) Schematic diagrams and the reaction mechanism of as-assembled LFP|Li/IBP-Cu|LFP pouch cell. (b) Galvanostatic discharge/charge profiles of LFP|Li/IBP-Cu|LFP pouch cell at 1 C. (c) Cycling performance and Coulombic efficiencies of LFP|Li/IBP-Cu|LFP pouch cell at 1 C. Photographs of a timer powered by LFP|Li/IBP-Cu|LFP pouch cell upon (d) bending, (e) flat states, and (f-g) long-term endurance test.

3. Conclusion

In summary, we developed an integrated bidirectional porous Cu current collector via a scalable powder-sintering strategy for improving the performances of Li metal batteries. The IBP-Cu with a well-interconnected skeleton improves the electrolyte wettability and ensures the homogeneous electric field and Li^+ concentration distribution, leading to a uniform Li deposition. Moreover, the IBP-Cu current collector maintains the through-pore structure during the Li plating/stripping process, providing a large surface for the Li accommodation and mitigating the volume change. Consequently, the Li/IBP-Cu anode exhibits extraordinary structure stability over 4000 h under 1.0 mA cm^{-2} and 1.0 mAh cm^{-2}. The fabricated coin cell with Li/IBP-Cu anode and $LiFePO_4$ cathode also show improved electrochemical performance in capacity, rate capability, and cycling performance compared to the cell with Li/PL-Cu anode. Most importantly, the LFP|Li/IBP-Cu|LFP pouch cell with IBP-Cu as bidirectional current collector significantly increases the anode utilization and results in a much higher improvement of energy density (~187.5%) than LFP|Li/IBP-Cu pouch cell. Such a facile and scalable method for producing integrated bidirectional porous Cu film provides us a homogeneous Li deposition current collector and the opportunity for increasing the device energy density by elevating the anode utilization.

Supporting Information

Supporting Information is available from the Wiley Online Library or from the author.

Acknowledgements

This work is jointly supported by NSFC (91963119, 51772157, 51802161, 52102265, 22179064, 21805140), China Postdoctoral Science Foundation (2020M681681), Jiangsu Provincial NSF (BK20210604), Research Startup Fund from NJUPT (NY220069, NY220085), and Science and Technology Innovation Project for Overseas Students of Nanjing, Priority Academic Program Development of Jiangsu Higher Education Institutions, State Key Laboratory of Organic Electronics and

Information Display, Jiangsu National Synergetic Innovation Center for Advanced Materials (SICAM). Q. Liang acknowledges the financial support from Australian Research Council (DE190100445).

Received: ((will be filled in by the editorial staff))
Revised: ((will be filled in by the editorial staff))
Published online: ((will be filled in by the editorial staff))

References

[1] H. Chen, Y. Yang, D. T. Boyle, Y. K. Jeong, R. Xu, L. S. de Vasconcelos, Z. Huang, H. Wang, H. Wang, W. Huang, *Nat. Energy* **2021**, 1-9.

[2] S. C. Kim, X. Kong, R. A. Vilá, W. Huang, Y. Chen, D. T. Boyle, Z. Yu, H. Wang, Z. Bao, J. Qin, *J. Am. Chem. Soc.* **2021**, 143 (27), 10301-10308.

[3] Z. Luo, X. Qiu, C. Liu, S. Li, C. Wang, G. Zou, H. Hou, X. Ji, Nano Energy **2020**, 105507.

[4] X. Shen, R. Zhang, X. Chen, X. B. Cheng, X. Li, Q. Zhang, *Adv. Energy Mater.* **2020**, *10 (10)*, 1903645.

[5] T. Zhang, H. Lu, J. Yang, Z. Xu, J. Wang, S.-i. Hirano, Y. Guo, C. Liang, *ACS Nano* **2020**, *14 (5)*, 5618-5627.

[6] L. Fu, M. Wan, B. Zhang, Y. Yuan, Y. Jin, W. Wang, X. Wang, Y. Li, L. Wang, J. Jiang, *Adv. Mater.* **2020**, *32 (29)*, 2000952.

[7] B. Han, D. Xu, S. S. Chi, D. He, Z. Zhang, L. Du, M. Gu, C. Wang, H. Meng, K. Xu, *Adv. Mater.* **2020**, *32 (42)*, 2004793.

[8] Y. Liu, X. Yin, X. Shen, P. Zou, X. Qin, C. Yang, Q. Zhang, F. Kang, G. Chen, B. Li, *Adv. Funct. Mater.* **2020,** *30 (38)*, 2002522.

[9] K. Tantratian, D. Cao, A. Abdelaziz, X. Sun, J. Sheng, A. Natan, L. Chen, H. Zhu, *Adv. Energy Mater.* **2020**, *10 (5)*, 1902819.

[10] D. Wang, C. Qin, X. Li, G. Song, Y. Liu, M. Cao, L. Huang, Y. Wu, *iScience* **2020**, *23 (1)*, 100781.

[11] X. Wang, G. Pawar, Y. Li, X. Ren, M. Zhang, B. Lu, A. Banerjee, P. Liu, E. J. Dufek, J.-G. Zhang, *Nat. Mater.* **2020**, *19 (12)*, 1339-1345.

[12] G. Yasin, M. Arif, T. Mehtab, X. Lu, D. Yu, N. Muhammad, M. T. Nazir, H. Song, *Energy Storage Mater.* **2020**, *25*, 644-678.

[13] J. Zheng, M. S. Kim, Z. Tu, S. Choudhury, T. Tang, L. A. Archer, *Chem. Soc. Rev.* **2020**, *49 (9)*, 2701-2750.

[14] R. Liu, W. Liu, Y. Bu, W. Yang, C. Wang, C. Priest, Z. Liu, Y. Wang, J. Chen, Y. Wang, *ACS Nano* **2020**, *14 (12)*, 17308-17320.

[15] Z. Lyu, G. J. Lim, R. Guo, Z. Kou, T. Wang, C. Guan, J. Ding, W. Chen, J. Wang, *Adv. Funct. Mater.* **2019**, *29 (1)*, 1806658.

[16] F. Qiu, S. Ren, X. Mu, Y. Liu, X. Zhang, P. He, H. Zhou, *Energy Storage Mater.* **2020**, *26*, 443-447.

[17] H. Xia, Q. Xie, Y. Tian, Q. Chen, M. Wen, J. Zhang, Y. Wang, Y. Tang, S. Zhang, *Nano Energy* **2021**, *84*, 105877.

[18] S. Xia, X. Zhang, C. Liang, Y. Yu, W. Liu, *Energy Storage Mater.* **2020**, *24,* 329-335.

[19] X. Yu, A. Manthiram, *Small Struct.* **2020**, *1 (2)*, 2000027.

[20] W. Zhao, Y. Lei, Y. Zhu, Q. Wang, F. Zhang, X. Dong, H. N. Alshareef, *Nano Energy* **2021**, *86*, 106120.

[21] L. Zhou, D. L. Danilov, R. A. Eichel, P. H. Notten, *Adv. Energy Mater.* **2021**, *11 (15)*, 2001304.

[22] C. Fang, J. Li, M. Zhang, Y. Zhang, F. Yang, J. Z. Lee, M.-H. Lee, J. Alvarado, M. A. Schroeder, Y. Yang, *Nature* **2019**, *572 (7770)*, 511-515.

[23] J. Holoubek, H. Liu, Z. Wu, Y. Yin, X. Xing, G. Cai, S. Yu, H. Zhou, T. A. Pascal, Z. Chen, *Nat. Energy* **2021**, *6 (3)*, 303-313.

[24] C. Jin, T. Liu, O. Sheng, M. Li, T. Liu, Y. Yuan, J. Nai, Z. Ju, W. Zhang, Y. Liu, *Nat. Energy* **2021**, *6 (4)*, 378-387.

[25] S.-Y. Lang, Z.-Z. Shen, X.-C. Hu, Y. Shi, Y.-G. Guo, F.-F. Jia, F.-Y. Wang, R. Wen, L.-J. Wan, *Nano Energy* **2020**, *75*, 104967.

[26] C. Niu, D. Liu, J. A. Lochala, C. S. Anderson, X. Cao, M. E. Gross, W. Xu, J.-G. Zhang, M. S. Whittingham, J. Xiao, *Nat. Energy* **2021**, *6 (7)*, 723-732.

[27] C. Fu, Y. Ma, S. Lou, C. Cui, L. Xiang, W. Zhao, P. Zuo, J. Wang, Y. Gao, G. Yin, *J. Mater. Chem. A* **2020**, *8 (4)*, 2066-2073.

[28] L. P. Hou, X. Q. Zhang, B. Q. Li, Q. Zhang, *Angew. Chem. Int. Ed.* **2020**, *132 (35)*, 15221-15225.

[29] H. Wang, Z. Yu, X. Kong, W. Huang, Z. Zhang, D. G. Mackanic, X. Huang, J. Qin, Z. Bao, Y. Cui, *Adv. Mater.* **2021**, 2008619.

[30] Q. Zhang, S. Liu, Z. Lin, K. Wang, M. Chen, K. Xu, W. Li, *Nano Energy* **2020**, *74,* 104860.

[31] F. Zhao, Q. Sun, C. Yu, S. Zhang, K. Adair, S. Wang, Y. Liu, Y. Zhao, J. Liang, C. Wang, *ACS Energy Lett.* **2020**, *5 (4),* 1035-1043.

[32] C. Cui, C. Yang, N. Eidson, J. Chen, F. Han, L. Chen, C. Luo, P. F. Wang, X. Fan, C. Wang, *Adv. Mater.* **2020**, *32 (12),* 1906427.

[33] Y. Jiang, B. Wang, P. Liu, B. Wang, Y. Zhou, D. Wang, H. Liu, S. Dou, *Nano Energy* **2020**, 105308.

[34] X. Liu, J. Liu, T. Qian, H. Chen, C. Yan, *Adv. Mater.* **2020**, *32 (2)*, 1902724.

[35] Z. Lu, W. Li, Y. Long, J. Liang, Q. Liang, S. Wu, Y. Tao, Z. Weng, W. Lv, Q. H. Yang, *Adv. Funct. Mater.* **2020**, *30 (7)*, 1907343.

[36] F. Liu, L. Wang, Z. Zhang, P. Shi, Y. Feng, Y. Yao, S. Ye, H. Wang, X. Wu, Y. Yu, Advanced Functional Materials 2020, 30, 2001607.

[37] W. Zhang, Z. Shen, S. Li, L. Fan, X. Wang, F. Chen, X. Zang, T. Wu, F. Ma, Y. Lu, *Adv. Funct. Mater.* **2020**, *30 (39)*, 2003800.

[38]Y. J. Gong, J. W. Heo, H. Lee, H. Kim, J. Cho, S. Pyo, H. Yun, H. Kim, S. Y. Park, J. Yoo, *Adv. Energy Mater.* **2020**, *10 (27)*, 2001479.

[39] Z. Hu, F. Liu, J. Gao, W. Zhou, H. Huo, J. Zhou, L. Li, *Adv. Funct. Mater.* **2020**, *30 (5)*, 1907020.

[40] X. Li, L. Yuan, D. Liu, M. Liao, J. Chen, K. Yuan, J. Xiang, Z. Li, Y. Huang, *Adv. Funct. Mater.* **2021**, *31 (18),* 2100537.

[41] Y. Zhong, F. Lin, M. Wang, Y. Zhang, Q. Ma, J. Lin, Z. Feng, H. Wang, *Adv. Funct. Mater.* **2020**, *30 (10),* 1907579.

[42] H. Shen, F. Qi, H. Li, P. Tang, X. Gao, S. Yang, Z. Hu, Z. Li, J. Tan, S. Bai, *Adv. Funct. Mater.* **2021**, 2103309.

[43] C. Wei, H. Fei, Y. Tian, Y. An, H. Guo, J. Feng, Y. Qian, *Energy Storage Mater.* **2020**, *26,* 223-233.

[44] Y. Jiang, J. Jiang, Z. Wang, M. Han, X. Liu, J. Yi, B. Zhao, X. Sun, J. Zhang, *Nano Energy* **2020**, *70*, 104504.

[45] W. Ye, F. Pei, X. Lan, Y. Cheng, X. Fang, Q. Zhang, N. Zheng, D. L. Peng, M. S. Wang, *Adv. Energy Mater.* **2020**, *10 (7),* 1902956.45.

[46] X. Gao, X. Yang, K. Adair, X. Li, J. Liang, Q. Sun, Y. Zhao, R. Li, T. K. Sham, X. Sun, *Adv. Energy Mater.* **2020**, *10 (7),* 1903753.

[47] J. Gu, Q. Zhu, Y. Shi, H. Chen, D. Zhang, Z. Du, S. Yang, *ACS Nano* **2020**, *14 (1)*, 891-898.

[48] T. Liu, Z. Shi, H. Li, W. Xue, S. Liu, J. Yue, M. Mao, Y. s. Hu, H. Li, X. Huang, *Adv. Mater.* **2021**, 2102034.

[49] H. Zhang, S. Ju, G. Xia, D. Sun, X. Yu, *Adv. Funct. Mater.* **2021**, *31 (16),* 2009712.

[50] S.-S. Chi, Q. Wang, B. Han, C. Luo, Y. Jiang, J. Wang, C. Wang, Y. Yu, Y. Deng, *Nano Lett.* **2020**, *20 (4)*, 2724-2732.

[51] Y. Liu, Y. Zhai, Y. Xia, W. Li, D. Zhao, *Small Struct.* **2021**, *2 (5),* 2000118.

[52] Z. Wang, X. Li, Y. Chen, K. Pei, Y.-W. Mai, S. Zhang, J. Li, *Chem* **2020**, *6 (11),* 2878-2892.

[53] T. Yang, Y. Sun, T. Qian, J. Liu, X. Liu, F. Rosei, C. Yan, *Energy Storage Mater.* **2020**, *26,* 385-390.

[54] Y.-X. Zhan, P. Shi, X.-Q. Zhang, F. Ding, J.-Q. Huang, Z. Jin, R. Xiang, X. Liu, Q. Zhang, *Energy Technol.* **2021**, *9 (2),* 2000700.

[55] J. Chen, X. Xu, Q. He, Y. Ma, *Chem. Res. Chin. Univ.* **2020**, *36,* 386-401.

[56] J. Chen, J. Zhao, L. Lei, P. Li, J. Chen, Y. Zhang, Y. Wang, Y. Ma, D. Wang, *Nano Lett.* **2020**, *20 (5),* 3403-3410.

[57] G. J. Lim, Z. Lyu, X. Zhang, J. J. Koh, Y. Zhang, C. He, S. Adams, J. Wang, J. Ding, *J. Mater. Chem. A* **2020**, *8 (18),* 9058-9067.

[58] K. Lin, T. Li, S. W. Chiang, M. Liu, X. Qin, X. Xu, L. Zhang, F. Kang, G. Chen, B. Li, *Small* **2020**, *16 (37),* 2001784.

[59] J. Qian, S. Wang, Y. Li, M. Zhang, F. Wang, Y. Zhao, Q. Sun, L. Li, F. Wu, R. Chen, *Adv. Funct. Mater.* **2021**, *31 (7),* 2006950.

[60] Y. Zhou, X. Zhang, Y. Ding, J. Bae, X. Guo, Y. Zhao, G. Yu, *Adv. Mater.* **2020**, *32 (38),* 2003920.

[61] P. Zou, Y. Sui, H. Zhan, C. Wang, H. L. Xin, H.-M. Cheng, F. Kang, C. Yang, *Chem. Rev.* **2021**, *121 (10),* 5986-6056.

[62] H. Fan, Q. Dong, C. Gao, B. Hong, Y. Lai, *Mater. Lett.* **2019**, *234,* 69-73.

[63] Y. Wang, Z. Wang, D. Lei, W. Lv, Q. Zhao, B. Ni, Y. Liu, B. Li, F. Kang, Y.-B. He, *ACS Appl. Mater. Interface* **2018**, *10 (24),* 20244-20249.

An integrated bidirectional porous Cu (IBP-Cu) current collector with a through-pore structure is served as an ultra-stable Li metal anode host that exhibits outstanding bidirectional stripping and plating performance in a practical Li metal battery.

Jianyu Chen, Sijia Li, Xin Qiao, Yizhou Wang, Linna Lei, Zhiyang Lyu, Jin Zhao,* Yu Zhang, Ruiqing Liu, Qinghua Liang, and Yanwen Ma*

Integrated Porous Cu Host Induced High-Stable Bidirectional Li Plating/Stripping Behavior for Practical Li Metal Batteries

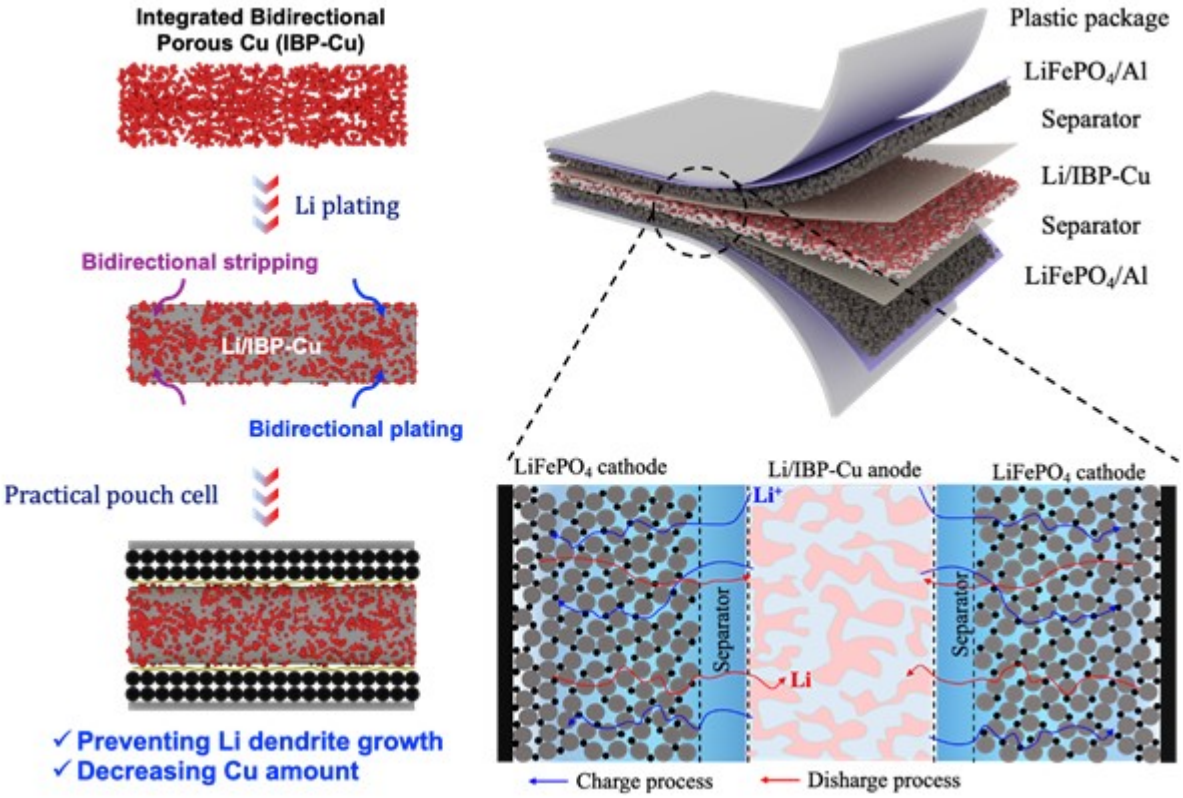

Author/s:
Chen, J;Li, S;Qiao, X;Wang, Y;Lei, L;Lyu, Z;Zhao, J;Zhang, Y;Liu, R;Liang, Q;Ma, Y

Title:
Integrated Porous Cu Host Induced High-Stable Bidirectional Li Plating/Stripping Behavior for Practical Li Metal Batteries

Date:
2022-02

Citation:
Chen, J., Li, S., Qiao, X., Wang, Y., Lei, L., Lyu, Z., Zhao, J., Zhang, Y., Liu, R., Liang, Q. & Ma, Y. (2022). Integrated Porous Cu Host Induced High-Stable Bidirectional Li Plating/Stripping Behavior for Practical Li Metal Batteries. SMALL, 18 (6), https://doi.org/10.1002/smll.202105999.